The EMBO Journal (2007) 26, 5143–5152 | © 2007 European Molecular Biology Organization | All Rights Reserved 0261-4189/07
www.embojournal.org

THE EMBO JOURNAL

Hyperphosphorylated tau in parahippocampal cortex impairs place learning in aged mice expressing wild-type human tau

Tetsuya Kimura, Shunji Yamashita, Tetsuya Fukuda, Jun-Mi Park, Miyuki Murayama, Tatsuya Mizoroki, Yuji Yoshiike, Naruhiko Sahara and Akihiko Takashima*

Laboratorty for Alzheimer's Disease, RIKEN Brain Science Institute, Wako, Saitama, Japan

To investigate how tau affects neuronal function during neurofibrillary tangle (NFT) formation, we examined the behavior, neural activity, and neuropathology of mice expressing wild-type human tau. Here, we demonstrate that aged (>20 months old) mice display impaired place learning and memory, even though they do not form NFTs or display neuronal loss. However, soluble hyperphosphorylated tau and synapse loss were found in the same regions. Mn-enhanced MRI showed that the activity of the parahippocampal area is strongly correlated with the decline of memory as assessed by the Morris water maze. Taken together, the accumulation of hyperphosphorylated tau and synapse loss in aged mice, leading to inhibition of neural activity in parahippocampal areas, including the entorhinal cortex, may underlie place learning impairment. Thus, the accumulation of hyperphosphorylated tau that occurs before NFT formation in entorhinal cortex may contribute to the memory problems seen in Alzheimer's disease (AD).

The EMBO Journal (2007) **26,** 5143–5152. doi:10.1038/sj.emboj.7601917; Published online 15 November 2007
Subject Categories: proteins; molecular biology of disease
Keywords: aging; learning and memory; Mn-enhanced MRI; Tau phosphorylation; transgenic mouse

Introduction

Because neurofibrillary tangles (NFTs) are present in various neurodegenerative diseases, including Alzheimer's disease (AD), and are observed in regions that display neuronal loss, NFT formation is thought to be a common mechanism underlying neurodegeneration (Gomez-Isla *et al*, 1997; Lee *et al*, 2001; Binder *et al*, 2005, Iqbal and Grundke-Iqbal, 2005; Takashima, 2006). The occurrence of tau mutations in frontotemporal dementia with parkinsonism-17 (FTDP-17) strongly supports the hypothesis that tau abnormalities induce the NFT formation and neuronal loss that ultimately lead to dementia (Goedert and Spillantini, 2000; Hutton, 2000; Spillantini *et al*, 2000). Therefore, studying and understanding the mechanisms underlying NFT formation may lead to new strategies for preventing tauopathy-associated dementias. With this thought in mind, researchers have generated transgenic (Tg) mice that express human tau with the FTDP-17 mutation (Gotz *et al*, 2000, 2001, 2004; Lewis *et al*, 2000, 2001; Ishihara *et al*, 2001; Tanemura *et al*, 2001, 2002; Tatebayashi *et al*, 2002; Egashira *et al*, 2005; Lee *et al*, 2005; Yoshiyama *et al*, 2005; Murakami *et al*, 2006). Indeed, these mice display NFTs, neuronal death, and behavioral deficits.

Another FTDP-17 mouse model displaying age-related NFTs, neuronal death, and behavioral deficits is the one that overexpresses P301L mutant tau under the regulation of a tetracycline-inducible promoter. Although the inhibition of mutant tau overexpression in these mice blocks neuronal death and improves memory, NFTs continue to form (Santacruz *et al*, 2005). This suggests that NFTs are not themselves toxic, but instead the mechanism of NFT formation is shared by the process underlying neuronal death and neuronal dysfunction (Ramsden *et al*, 2005; Santacruz *et al*, 2005; Spires *et al*, 2006). The relationship between neuronal loss and memory dysfunction in the P301L mutant tau mouse model remains unclear.

Although most mouse models of FTDP-17 mutant tau exhibit NFTs, neuronal loss, and behavioral deficits, one model does not: 12-month-old mice expressing mutant (N279K) tau display behavioral deficits but do not display NFTs and neuronal loss (Taniguchi *et al*, 2005). These findings suggest that behavioral deficits might occur before NFTs form and neuronal death occurs. These findings raised important questions: which affected brain region is responsible for age-related behavioral deficits? How does neuronal activity in this region vary with age? Which form of tau affects neuronal activity in this region?

Expression of FTDP-17 mutant tau in mouse brain indeed affects brain function, inducing behavioral deficits, neuronal loss, and NFT formation, suggesting that FTDP-17 mutant tau might form a specific fibrillar structure that causes these events. However, NFT formation, neuronal loss, and brain dysfunction are seen not only in FTDP-17 but also in AD, other age-related neurodegenerative diseases, and even in normal aging—all conditions not caused by tau mutations. This suggests that wild-type tau may form the same type of structure formed by FTDP-17 mutant tau. Indeed, one group showed that overexpression of wild-type human tau in mice induced NFT-like inclusions and neuronal loss (Ishihara *et al*, 2001), indicating that wild-type tau could contribute to NFT formation.

To understand tau-induced brain dysfunction in neurodegenerative disease and aging, we generated a Tg mouse line

*Corresponding author. Laboratory for Alzheimer's Disease, RIKEN Brain Science Institute, 2-1 Hirosawa, Wako, Saitama 351-0198, Japan. Tel: +81 48 467 9627; Fax: +81 48 467 5916;
E-mail: kenneth@brain.riken.jp

Received: 5 July 2007; accepted: 17 October 2007; published online: 15 November 2007

expressing wild-type human tau. To determine which brain region's activity is linked to impairment of place learning in this mouse model, we analyzed the relationship between age-dependent tau-induced changes in behavior and the corresponding activity in all brain regions using Mn-enhanced MRI (MEM) methods.

Results

Aged Tg mice expressing wild-type human 4 repeat tau (Wtau-Tg) exhibit hyperphosphorylated tau but no NFTs and neuronal loss

An 8.5 kb portion of the CaMK-II promoter containing upstream control regions and the transcriptional initiation site drives expression postnatally in forebrain neurons (Figure 1A). Western blot analysis using TauN antibody revealed that Wtau-Tg mice expressed human tau in hippocampus, neocortex, striatum, olfactory bulb, and thalamus (Figure 1). Exogenous tau expression was barely detectable in midbrain, cerebellum, and spinal cord. Hippocampus and neocortex showed higher expression levels compared with other regions (Figure 1B, 10-month-old mice). The highest levels of exogenous tau expression were three- to fivefold higher than those of endogenous tau. The pattern of exogenous tau expression was the same in adult (9–13 months old) and aged (20–24 months old) mice. Immunohistochemical analysis using anti-human tau antibody HT7 (Figure 1C) confirmed this regional expression pattern, selectively staining mainly forebrain neurons.

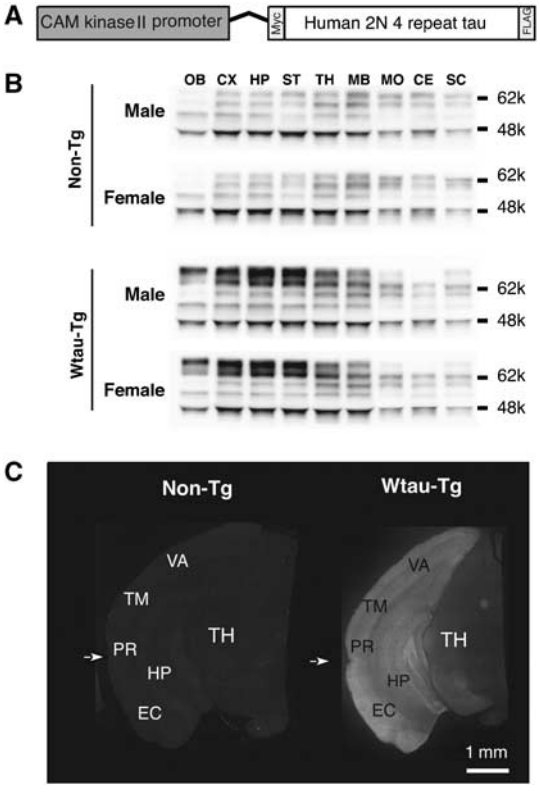

Figure 1 Generation of a transgenic mouse expressing wild-type human 2N/4 repeat tau. Expression of wild-type human 4 repeat tau tagged with myc and flag epitopes was regulated by the CAM kinase II promoter (**A**). The pattern of tau expression in different brain regions was determined by immunoblotting using anti-tauN antibody (**B**), which recognizes the N-terminus of tau, and by immunohistochemistry using human tau-specific anti-tau antibody HT7 (**C**). Male and female mice did not exhibit different expression patterns. OB, olfactory bulb; CE, cerebellum; CX, cerebral cortex; EA, entorhinal area; HP, hippocampus; MB, midbrain; MD, medulla; PIR, piriform area; rf, rhinal fissure; SC, spinal cord; ST, striatum; TA, temporal area; TH, thalamus; VA, visual area.

In Western blots of Tris-buffered saline (TBS)-soluble fractions derived from the brains of Wtau-Tg mice, immunoreactivity for AT8, AT180, PS262, and PHF1—antibodies that recognize tau phosphorylated at different serines and threonines—were examined. Immunoreactivity for AT180 and PHF1 increased with aging, whereas that for AT8 and PS262 did not change (Figure 2A–F). These results suggest that tau in the brains of Wtau-Tg mice took on additional hyperphosphorylation states with aging.

To examine whether these Tg mice form tau filaments, we purified insoluble tau with sarcosyl detergent and analyzed sarcosyl-insoluble fractions by Western blotting with anti-tau JM antibody. The sarcosyl-insoluble fractions derived from the brains of Wtau-Tg mice did not display positive tau signals (Figure 2H), whereas those derived from the brains of P301L FTDP-17 mutant human tau-expressing mice (JNPL3) (Lewis *et al*, 2000) exhibited strong anti-tau immunoreactivity, as expected. In TBS-soluble fractions, the overall tau expression levels in Wtau-Tg and female JNPL3 mice were almost the same in both adult and aged groups (Figure 2G). Taken together, these observations indicate that in the brains of Wtau-Tg mice tau became hyperphosphorylated with increasing age, but did not form tau aggregates that were biochemically similar to those comprising NFTs. Furthermore, in brain sections from Wtau-Tg mice stained with the Gallyas method, we did not observe any silver-stained neurons (Supplementary Figure 1B, D). Moreover, the wet weight of brains from Wtau-Tg and non-Tg mice did not differ, nor did neuron counts in the entorhinal and adjacent sensory cortices (Supplementary Figure 1E, F). These are consistent with GFAP immunoreactivity in Wtau-Tg and non-Tg mice, which was indistinguishable (Supplementary Figure 1A, B), because GFAP immunoreactivity reflects neuronal death. In summary, our Wtau-Tg mouse model showed hyperphosphorylation of tau but no NFT formation or neuronal loss.

Aged Wtau-Tg mice display impaired place learning

To investigate the effects of age-dependent hyperphosphorylated tau on brain function, we assessed place learning in adult and aged non-Tg and Wtau-Tg mice using the Morris water maze. Non-Tg and Wtau-Tg adult mice (9–13 months old) learned at a similar rate, as assessed by error scores (see Materials and methods) (Figure 3A; non-Tg mice, Friedman test, $P<0.0001$; Wtau-Tg mice, Friedman test, $P<0.0001$). Both non-Tg and Wtau-Tg mice stayed significantly longer in the target quadrant (Figure 3B; non-Tg mice, Friedman test, $P<0.0001$; Wtau-Tg mice, Friedman test, $P=0.0007$). In summary, adult non-Tg and Wtau-Tg mice did not significantly differ in place learning and memory (see two-way ANOVA results in Table I).

In contrast to the adult mice, aged non-Tg and Wtau-Tg mice (20–24 months old) differed significantly in learning, as assessed by the Morris water maze (Figure 3C; Table I). Error scores for non-Tg mice started to decrease after 4 days of learning, showing a significant reduction over the 9 days of

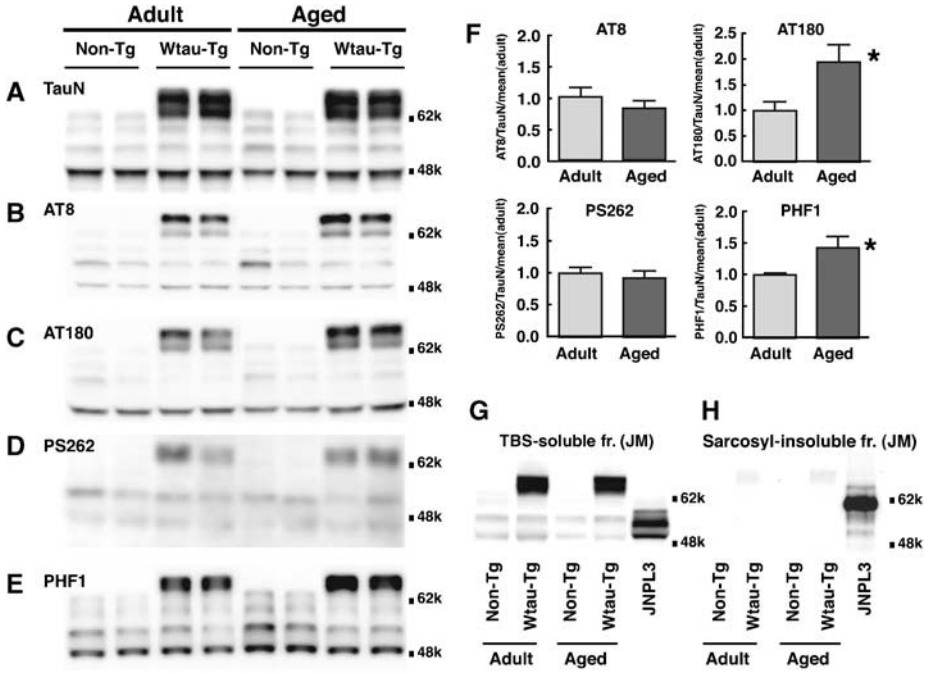

Figure 2 The brains of Wtau-Tg mice form hyperphosphorylated tau but do not form sarcosyl-insoluble tau aggregates. (**A–F**) Western blots of TBS-soluble fractions from the brain homogenates of 8-month-old (Adult) and 22-month-old (Aged) Wtau-Tg mice. Immunoblots were probed with various tau antibodies: (A) TauN, which recognizes total phosphorylation-independent tau; (B) AT8, which recognizes tau phosphorylated at Ser202 and Ser205; (C) AT180, which recognizes tau phosphorylated at Thr231; (D) PS262, which recognizes tau phosphorylated at Ser262; and (E) PHF1, which recognizes tau phosphorylated at Ser396 and Ser404. Quantitative analysis of immunoreactivity for AT8, AT180, PS262, and PHF1 in adult ($n=6$) and aged ($n=6$) Wtau-Tg mice. Immunoreactivity for each phospho-dependent antibody was normalized by that of phospho-independent antibody (TauN). The results are presented as relative intensity of normalized immunoreactivity in Wtau-Tg mouse (F) (*$P<0.05$; Student's *t*-test). (**G, H**) Western blots of TBS-soluble and sarcosyl-insoluble fractions from the brains of non-Tg and Wtau-Tg mice, and 11-month-old mice overexpressing P301L mutant tau (JNPL3) (positive control). Immunoblots were probed with anti-tau antibody JM, which recognizes phosphorylation-independent tau (i.e., total tau). Although the total tau levels in the TBS-soluble fractions were about the same in both types of mice (G). The brains of JNPL3 mice contained sarcosyl-insoluble tau aggregates, as expected, but the brains of aged Wtau-Tg mice did not (H).

testing (Friedman test, $P<0.0001$). In Wtau-Tg mice, however, error scores remained more or less constant throughout the entire test period (Friedman test, $P=0.0573$). In the probe test, the target quadrant search time for aged Wtau-Tg mice was not significantly different from the time spent in the other quadrants (Friedman test, $P=0.1040$), whereas the aged non-Tg mice spent a significantly longer time searching in the target quadrant (Friedman test, $P<0.0001$; Figure 3D). Swimming speed (motor control ability) and thigmotaxic tendency (emotional control ability) on the first day of training were not significantly different between non-Tg and Wtau-Tg mice (see Table II, ANOVA results), suggesting that these motor and emotional factors did not account for the group differences in the Morris water maze. Thus, aged Wtau-Tg mice are impaired in place learning and memory.

Analysis of neural activity using Mn-enhanced MRI

As manganese (Mn) enters into neurons through calcium channels and accumulates there, positive MR signals can be detected, allowing active regions of the mouse brain during behavior to be sampled with MRI (Wadghiri *et al*, 2004; Yu *et al*, 2005). We used MEM to identify which brain regions in aged Wtau-Tg mice are deficient, leading to place learning and memory impairment.

After confirming that the MR image reflected activity-dependent Mn incorporation into neurons under our protocol (Supplementary Figure 2), we investigated brain activity during place learning in non-Tg and Wtau-Tg mice. Aged Wtau-Tg mice clearly showed a lower MEM signal in the parahippocampal area in coronal (Figure 4A, C) and horizontal (Figure 4B, D) sections compared to non-Tg mice. To precisely compare neuronal activity in the parahippocampal region among adult and aged non-Tg and Wtau-Tg mice, we prepared flat maps of parahippocampal activity by averaging each regional MR signal of the parahipppocampal area using 4–6 mice (Figure 4E, F; see Materials and methods for details). Adult Wtau-Tg and non-Tg mice showed almost the same pattern of activity on flat map representations. Aged Wtau-Tg mice exhibited reduced activity in perirhinal cortex, postrhinal cortex, and lateral and medial entorhinal cortices, whereas non-Tg mice exhibited the same activity as that of adults. Thus, reduced neural activity in perirhinal and lateral and medial entorhinal cortices of aged Wtau-Tg mice may underlie the place learning and memory deficits we observed.

The next question we asked is which region(s) of neural activity correlate best with memory performance in the Morris water maze test? We calculated correlations between neural activity on the flat map and the corresponding index of place memory for each animal. The linear correlation coefficient between each pixel data on the flat map and memory index was calculated for the two aged mice groups (6 non-Tg and 4 Wtau-Tg mice). Figure 5 shows the correlation map for the MEM signal of each pixel and the memory index. Higher

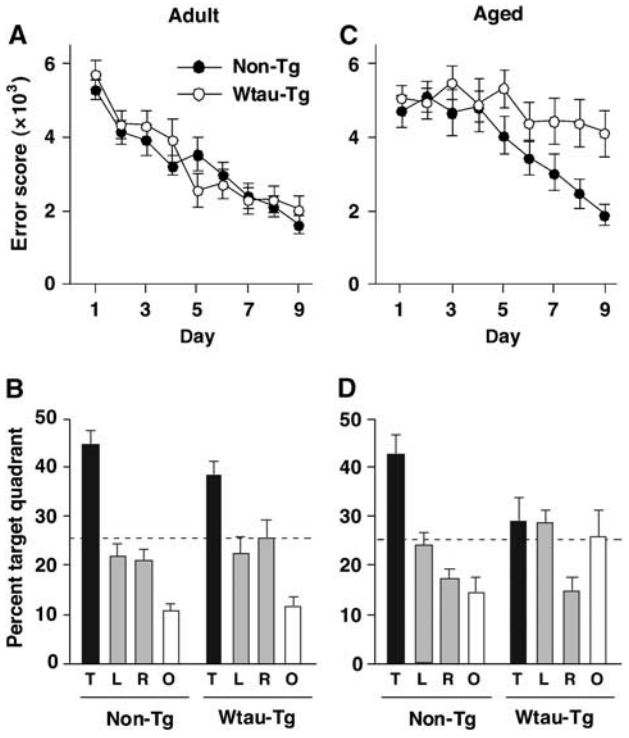

Figure 3 Impairment of place learning and memory in aged Wtau-Tg mice. The Morris water maze was used to assess place learning and memory of adult (9–13 months old) non-Tg ($n=23$) and Wtau-Tg ($n=14$) mice, and aged (20–24 months old) non-Tg ($n=12$) and Wtau-Tg ($n=13$) mice. Results expressed as means±s.e.m. Learning is expressed as error scores (**A, C**), and memory performance is expressed as a percentage of total time spent in the target quadrant during the probe test (**B, D**); the probe test was given on the 10th day of the experiment (see Materials and methods). Learning curves and memory performance of adult non-Tg and Wtau-Tg mice were not significantly different (A, B). By contrast, aged Wtau-Tg mice took significantly longer than non-Tg mice to learn the task ($P<0.0001$, $F=16.19$) (C). Memory performance in aged Wtau-Tg mice was also worse than that of non-Tg mice ($P=0.0040$, $F=4.742$) (D).

Table I Learning speed and learning performance

	Adult		Aged	
	Non-Tg	Wtau-Tg	Non-Tg	Wtau-Tg
Adult				
Non-Tg ($n=23$)		$P=0.219$[b] ($F=1.493$)	$P=0.444$[b] ($F=0.898$)	$P<0.001$[b] ($F=10.31$)
Wtau-Tg ($n=14$)	$P=0.570$[a] ($F=0.322$)		$P=0.123$[b] ($F=1.971$)	$P=0.0007$[b] ($F=6.172$)
Aged				
Non-Tg ($n=12$)	$P=0.004$[a] ($F=8.416$)	$P=0.036$[a] ($F=4.461$)		$P=0.004$[a] ($F=4.742$)
Wtau-Tg ($n=13$)	$P<0.001$[a] ($F=57.34$)	$P<0.001$[a] ($F=37.53$)	$P<0.001$[a] ($F=1.6.19$)	

[a]Learning speed.
[b]Learning performance.

Table II Motor and emotional control ability

	Genotype[a]		Two-way ANOVA results	
	Non-Tg	Wtau-Tg	Non-Tg	Wtau-Tg
Speed (cm/s)				
Adult	13.8±3.2	15.3±2.7	$P<0.0001$ ($F=21.46$)	$P=0.2475$ ($F=1.36$)
Aged	10.6±3.5	11.0±3.0		
Thigmotaxis (%)				
Adult	52.7±12.8	58.7±11.6	$P<0.0001$ ($F=18.91$)	$P=0.1308$ ($F=2.35$)
Aged	39.6±15.1	43.6±9.9		

[a]Mean±s.e.

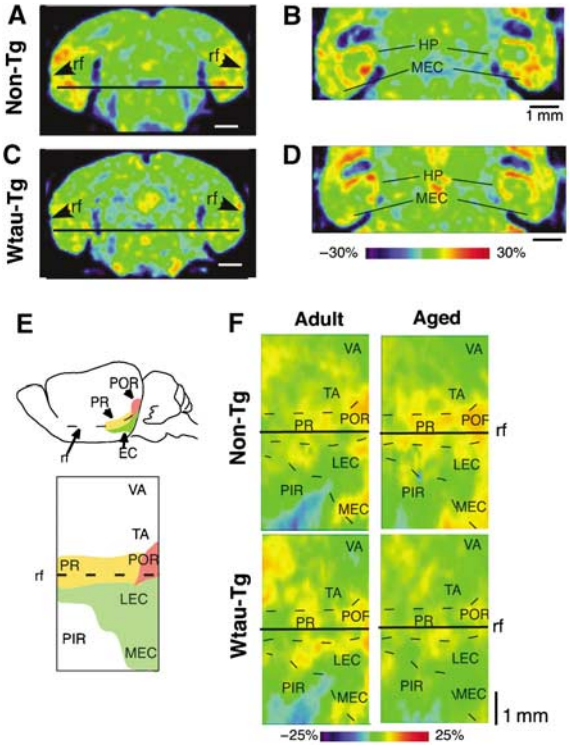

Figure 4 MEM analysis of neural activity in non-Tg and Wtau-Tg mice. (**A–D**) Coronal (A, C) and horizontal brain sections (B, D) showing neural activity in hippocampal and parahippocampal regions. The horizontal lines in (A) and (C) show the dorsoventral level at which the horizontal views in (B) and (D) were acquired. The relative intensity of MEM signals is shown as color spectrum change by normalizing these intensities by the mean signal intensity in the dorsal striatum. In the Wtau-Tg mouse, the MEM signal in the medial entorhinal cortex was weaker than that in the non-Tg mouse. At this level, signals in the hippocampus (HP) were not noticeably different. (**E**) Representative two-dimensional flat map (lower panel) of the parahippocampal region of the mouse brain. The yellow, red, and green areas shown on a lateral view of the mouse brain (top panel) correspond to perirhinal (PR), postrhinal (POR), and entorhinal (EC) cortices in the flat map. The map was generated as described in Materials and methods. (**F**) Four flat maps showing averaged MRI signals from adult (9–13 months old) non-Tg ($n=4$) and Wtau-Tg ($n=5$) mice, and aged (20–24 months old) non-Tg ($n=6$) and Wtau-Tg ($n=4$) mice. The animals used in this analysis were randomly selected. rf, rhinal fissure; LEC, lateral entorhinal cortex; MEC, medial entorhinal cortex; PIR, piriform cortex; TA, temporal area; VA, visual area.

correlations were observed for the caudal parahippocampal region. The correlation coefficient (R^2) was 0.7089 for the lateral entorhinal cortex, 0.7524 for the medial entorhinal cortex, 0.8000 for the postrhinal cortex, and 0.8301 for the temporal area. The correlation coefficient of neural activity and memory index in visual cortex was less than 0.5, which indicates no significant correlation. Therefore, the reduction

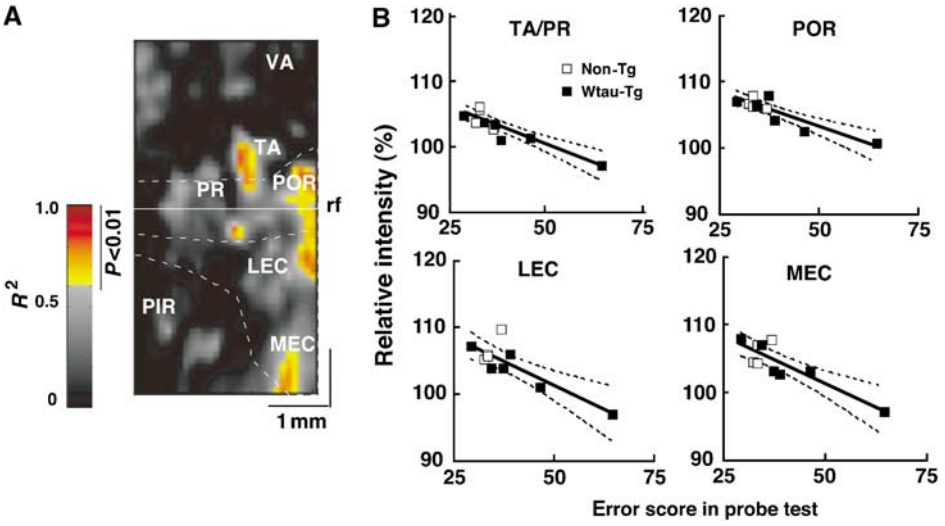

Figure 5 Correlation between regional neural activity and memory performance. (**A**) Pseudocolored flat map showing the coefficients of determination (R^2) of MEM signals in different parahippocampal regions as a function of memory performance score in aged mice. This map is based on flat maps showing the regional distribution of MEM signals during place learning. The red-to-yellow–colored areas in the map represent areas showing significant negative correlation between neural activity and memory performance ($P<0.01$, Pearson's correlation test). (**B**) Correlation curves for temporal area (TA), perirhinal area (PR), lateral entorhinal cortex (LEC), and medial entorhinal cortex (MEC). rf, rhinal fissure; PIR, piriform; POR, postrhinal area; VA, visual area. A full colour version of this figure is available at *EMBO Journal* Online.

of neural activity in the caudal parts of the parahippocampal region—postrhinal cortex, lateral entorhinal cortex, and medial entorhinal cortex—might cause place learning and memory impairment in aged Wtau-Tg mice in the absence of NFT formation.

Aged Wtau-Tg mice display enhanced PHF1-site phosphorylation of tau in layer II of the entorhinal cortex

To determine which tau phosphorylation state affects neural activity in the entorhinal cortex of aged mice, we immunostained coronal brain sections with (1) H150, which recognizes phosphorylation-independent human tau (2) AT8, which recognizes phosphorylation of tau at Ser202 and Ser205 and (3) PHF1, which recognizes phosphorylation of tau at Ser396 and Ser404. In adult and aged Wtau-Tg mice, H150 and AT8 immunoreactivity was comparable and observed throughout the forebrain (Figure 6; Supplementary Figure 4 for whole brain). PHF1 immunoreactivity, however, differed between adult and aged mice. In entorhinal cortex, few PHF1-positive neurons were observed in adult mice, but robust PHF1 immunoreactivity, especially in layer II, was observed in aged mice (Supplementary Figure 4 for whole brain). On the other hand, in visual cortex (VA), an area where neural activity and memory performance was uncorrelated, few PHF1-positive neurons were seen in adult and aged mice. AT8 and H150 immunoreactivity was comparable in the VA of both mice. Immunoreactivity of PSD95, a postsynaptic marker, in layer II neurons of entorhinal cortex was clearly reduced in aged Wtau-Tg mice compared with that in adult and aged non-Tg and in adult Wtau-Tg mice (Figure 7A, B). This synapse loss was confirmed by Golgi staining (Figure 7C). In aged Wtau-Tg mice, the number of dendritic spines was reduced compared with that in aged non-Tg mice. These results suggested that layer II neurons of entorhinal cortex exhibited tau hyperphosphorylation and synapse loss with aging. These histochemical findings show

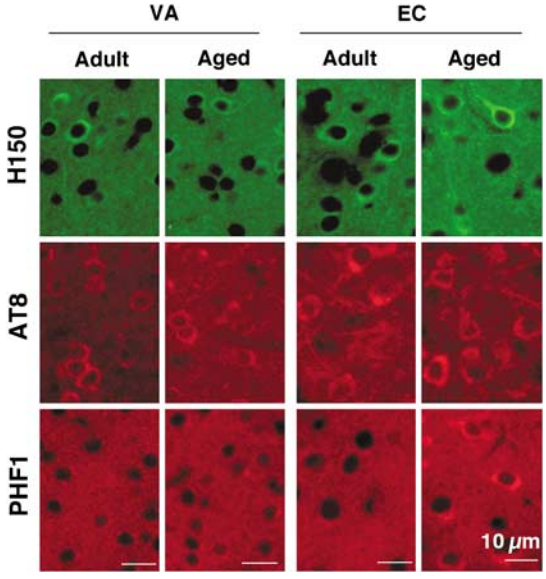

Figure 6 Distribution of phosphorylated tau in adult and aged Wtau-Tg mouse brains. Coronal brain sections immunostained with H150, a phosphorylation-independent anti-tau antibody; AT8, an antibody that recognizes tau phosphorylated at Ser202 and Ser205; and PHF1, an antibody that recognizes tau phosphorylated at Ser396 and Ser404 (Supplementary Figure 4). Magnified images of PHF1 immunoreactivity in visual area (VA) and entorhinal cortex (EC) are shown.

that PHF1 immunoreactivity in the entorhinal cortex increased with age, whereas AT8 immunoreactivity did not, suggesting that additional phosphorylation of tau at the PHF1 site might induce neural dysfunction due to synaptic loss that ultimately leads to impaired place learning and memory.

To compare neural activity with PHF1 immunoreactivity in brain regions that corresponded to memory impairment, we generated two-dimensional flat maps showing the distribu-

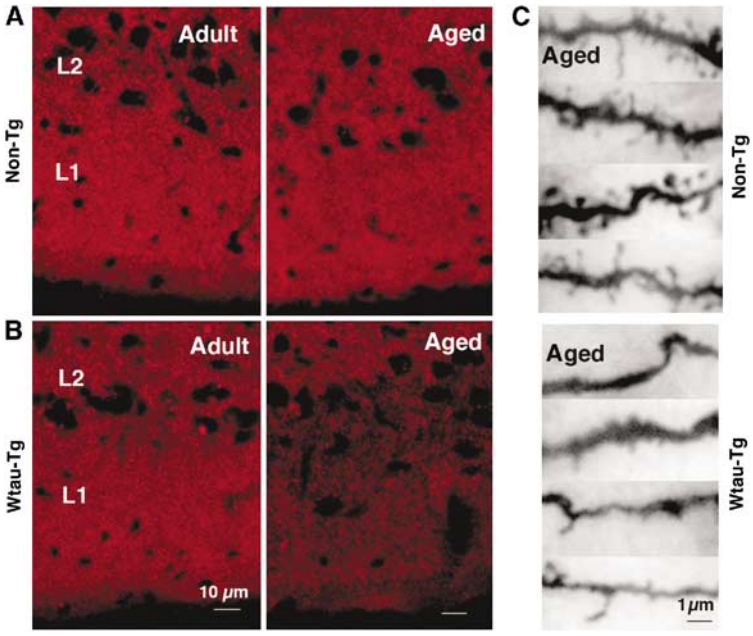

Figure 7 Synapse loss among layer II entorhinal cortex neurons in aged Wtau-Tg mice. Coronal brain sections immunostained with antibodies against the postsynaptic marker PSD95 in non-Tg (**A**) and Wtau-Tg (**B**) mice. L1, layer I of entorhinal cortex; L2, layer II of entorhinal cortex. Left panels contain images of brain sections from adult non-Tg and Wtau-Tg mice; right panels contain images of brain sections from aged non-Tg and Wtau-Tg mice. (C) Golgi staining shows dendritic spines of entorhinal cortical layer II neurons of aged non-Tg (top panel) and aged Wtau-Tg (bottom panel) mice.

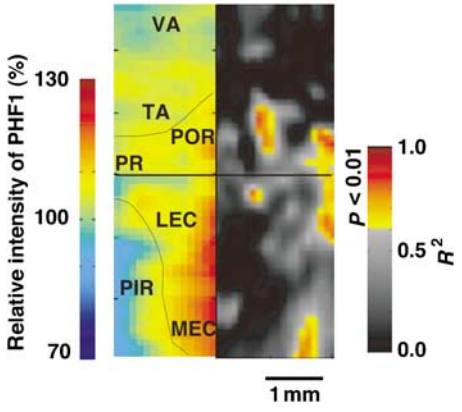

Figure 8 Parahippocampal cortical flat maps showing the distribution and intensity of PHF1 immunoreactivity (left) and MRI signal intensity as a function of memory performance (right). PHF1-immunostaining intensity in the parahippocampal region was normalized by PHF1-immunostaining intensity in either the parietal or visual areas in each section. The map in the right panel was reproduced from Figure 5. It shows the distribution of significant correlation between neural activity and memory index. rf, rhinal fissure; LEC, lateral entorhinal cortex; MEA, medial entorhinal cortex; PIR, piriform cortex; POR, postrhinal cortex; PR, perirhinal cortex; VA, visual area.

tion and intensity of PHF1 immunoreactivity and compared these maps to maps showing neural activity as a function of memory index (Figure 8). The distribution of PHF1 immunoreactivity in parahippocampal regions corresponded to areas of increased memory impairment. The elevated phosphorylation of tau at the PHF1 epitope may underlie the age-dependent memory impairment we observed in Wtau-Tg mice. Thus, hyperphosphorylated tau, including tau phosphorylated at AT8 and PHF1 sites, but not insoluble tau, may cause tau-induced neural dysfunction in the entorhinal cortex, ultimately leading to impaired place learning and memory.

Discussion

One goal of AD research is to determine the cause of memory deficits and dementia. Today, many AD animal models exist that exhibit β-amyloid deposition and/or NFT formation. Some of these models show memory impairments (Chapman *et al*, 1999; Chen *et al*, 2000; Lalonde *et al*, 2002; Tanemura *et al*, 2002; Tatebayashi *et al*, 2002; Oddo *et al*, 2003; Van Dam *et al*, 2003; Santacruz *et al*, 2005). However, the mechanisms underlying memory impairment associated with NFT formation and/or β-amyloid deposition remain unclear. In the present study, MEM clearly indicates that in Wtau-Tg mice reduced neural activity in the entorhinal cortex correlates well with the memory index. In the entorhinal cortex, tau was highly phosphorylated, at least at the AT8- and PHF1-immunoreactive sites, but insoluble tau aggregates did not form. Thus, our results suggest that hyperphosphorylated tau, but not insoluble tau, might affect neural activity. Although endogenous tau-deficient mice expressing six isoforms of human wild-type tau form NFTs and show NFT-like pathology (Andorfer *et al*, 2005), our mice, which express the longest form of human wild-type tau, did not show NFT-like pathology. One possible explanation for these two disparate observations is that the mice in the study by Andorfer *et al* (2005) did not express endogenous mouse tau, whereas our mice did. Thus, endogenous tau may have inhibited the formation of NFT-like pathology in Wtau-Tg mouse brains.

Tau in AD is abnormally hyperphosphorylated at over 30 sites. A recent study has shown Thr231 (AT180 site) and Ser262 (PS262) to be among the major pathogenic phosphorylation sites (Wang *et al*, 2007). We examined tau phosphorylation in Wtau-Tg mice (Supplementary Figure 5) and found that 14 tau phosphorylation sites showed positive signals. Therefore, most sites on tau were phosphorylated in Wtau-Tg mice. Quantitative analysis of tau phosphorylation indicated that phosphorylation of the PHF1 and Thr231 (AT180) sites increased with aging, but phosphorylation of the Ser262 and AT8 sites did not. Because some tau localized to cytoplasm when overexpressed and because tau phosphorylated at Ser262 lost its ability to bind to microtubules, cytoplasmic tau may represent tau phosphorylated at both Ser262and AT8 sites, the phosphorylation of which occurs independently of aging in case of tau overexpression. In addition to this type of phosphorylation scenario, some sort of aging-related factor may induce the hyperphosphorylation of PHF1 and AT180 sites in neurons of the entorhinal cortex. Therefore, tau phosphorylation may play two roles during neurodegeneration. One is to detach tau from microtubules (phosphorylation of AT8 and PS262 sites), which occurs in Wtau-Tg mice in an age-independent manner, and the other is to induce neural dysfunction by additional phosphorylation (of PT231 and PHF1 sites), which occurs in an age-dependent manner. Consequently, hyperphosphorylated tau may induce retrograde neuronal degeneration (Iqbal and Grundke-Iqbal, 2005) via synapse loss.

Santacruz *et al* (2005) reported that in rTg(tau P301L)4510 mice, which express P301L mutant tau, inhibition of mutant tau overexpression during the disease state blocked neuronal death and improved memory. Nonetheless, these mice still produced NFTs. This report suggested that neuronal loss and memory impairment might occur before NFT formation. However, Santacruz *et al* (2005) did not clarify the relationship between neuronal death and memory impairment. In our study, we observed no gliosis indicative of neuronal death and very few Gallyas silver-stained neurons indicative of NFT formation in aged Wtau-Tg mice, supporting the hypothesis that tau-induced memory impairment occurs in the absence of neuronal loss and NFT formation. Thus, tau-induced neuronal dysfunction may not be due to neuronal death and NFT formation.

Mandelkow's group reported that tau overexpression affects axonal transport by obstructing kinesin movement on microtubules (Ebneth *et al*, 1998; Seitz *et al*, 2002; Stamer *et al*, 2002; Santarella *et al*, 2004). Indeed, in Wtau-Tg mice, we found that the levels of tau associated with microtubules were greater than those in non-Tg mice (data not shown). If this increase in tau-microtubule binding causes neural dysfunction, even adult Wtau-Tg mice should display behavioral deficits. However, both adult Wtau-Tg and non-Tg mice showed comparable learning and memory abilities. Learning and memory impairment was observed only in Wtau-Tg mice that were old, an age at which the level of tau-microtubule binding was the same as that in adult mice. Therefore, the learning and memory impairment in Wtau-Tg mice might not be simply due to tau overexpression, but may occur through another mechanism.

Our previous study demonstrated that the number of granular tau aggregates, an intermediate form of tau fibril, increases in prefrontal cortex far before NFTs form (Maeda *et al*, 2006, 2007), which was found in AD brain (Iqbal *et al*, 1986; Bancher *et al*, 1989; Kopke *et al*, 1993). Granular tau aggregates are composed of hyperphosphorylated tau, including tau phosphorylated at the PHF1 epitope, and are recovered in the sarcosyl-soluble fraction. If the working memory impairment that occurs during aging (Rypma *et al*, 2001; Hedden and Gabrieli, 2004, 2005) is caused by formation of granular tau aggregates in prefrontal cortex, then we would expect to find increased levels of highly phosphorylated tau and granular tau aggregates in Wtau-Tg. Indeed, highly phosphorylated tau may form toxic aggregates, which in turn may impair neuronal function. This premise is consistent with the findings of Alonso and co-workers who recently discovered that a soluble form of hyperphosphorylated tau called ADP tau sequesters normal tau, MAP1, and MAP2 from microtubules, causing the microtubules to collapse (Alonso *et al*, 1994, 1996, 1997, 2006), and with our previous observations that neurons accumulating hyperphosphorylated tau are not immunoreactive for tubulin (Tanemura *et al*, 2001, 2002; Tatebayashi *et al*, 2002). Thus, the accumulation of hyperphosphorylated tau might affect microtubule stability, leading to neuronal dysfunction due to synaptic loss and consequently inducing retrograde neurodegeneration, neuronal death, or NFT formation. Nevertheless, the precise biochemical relationship between the accumulation of hyperphosphorylated tau, neuronal dysfunction, NFT formation, and neuronal death needs to be clarified.

The entorhinal and hippocampal circuit is essential for the formation of place memory (Hafting *et al*, 2005; Steffenach *et al*, 2005; McNaughton *et al*, 2006). When navigating the Morris water maze, a mouse forms a place memory by acquiring context-based information about a target's location, which occurs mainly via entorhinal-hippocampal circuit-mediated learning (Morris, 2006). In our task, the learning process is represented by a learning curve, and the process of memory is reflected in performance on the probe test.

Certain AD mouse models and models of other neurodegenerative disorders show memory impairment, as demonstrated in the Morris water maze. However, because the brain region underlying memory impairment is unknown in most of these models, it is difficult to evaluate a connection between possible responsible proteins and neuronal dysfunction. MEM (Wadghiri *et al*, 2004; Yu *et al*, 2005) enabled us to identify the brain regions underlying memory impairment in Wtau-Tg mice: the parahippocampal region, especially the entorhinal cortex. As memories are formed through the relay of sensory information to the hippocampus through layer II of the entorhinal cortex, it is conceivable that entorhinal cortical dysfunction results in learning deficits and memory impairment. This premise is corroborated by our observation that entorhinal cortical MEM signals correlate well with memory indices.

Even during normal aging, NFTs form first in entorhinal cortex; and in AD, NFTs ultimately spread into limbic areas and isocortex after Aβ deposition (Braak and Braak, 1991), apparently causing dementia with memory impairment. In the present study, our aged Wtau-Tg mice showed significant place memory impairment due to reduced neural activity in parahippocampal regions, especially in the entorhinal cortex, without displaying NFTs and Aβ deposition. Thus, our mouse model may mimic what occurs in normal aging in humans, because both in Wtau-Tg mice and in humans tau affects

entorhinal activity first. Hyperphosphorylated tau, not insoluble tau aggregates, were prominently observed in layer II of the entorhinal cortex, the cell layer containing neurons that project to the dentate gyrus and CA3 (Lavenex and Amaral, 2000). This is consistent with our hypothesis that the memory impairment and reduced neural activity we observed in hippocampal and parahippocampal regions is due to the accumulation of hyperphosphorylated tau in these regions. Thus, preventing or reducing the accumulation of hyperphosphorylated tau in this animal model may lead to the development of potential treatments for tauopathies like AD. Detecting entorhinal cortical dysfunction early on may also be key to preventing tauopathies, including AD, from developing.

Materials and methods

Animals

Generation of Tg mouse lines expressing wild-type human tau was performed as described previously (Tanemura *et al*, 2002; Tatebayashi *et al*, 2002), except that the CaMK-II promoter was used for the expression. A cDNA construct of wild-type human tau containing myc (EQKLISEEDL) and FLAG (DYKDDDDK) tags at the N- and C-terminal ends, respectively, was inserted into a CaMK-II chain expression vector at the *Xho*I and sites. A 4.3-kb *Bgl*II–*Nae*I fragment containing the CaMK-II promoter–wild-type human tau cDNA and a 3′-untranslated sequence was used as the transgene to create the Wtau-Tg mice on a C57BL/6J background (Figure 1A).

Antibodies

We used the following antibodies: mouse monoclonal anti-myc (clone 9E10; Covance, Richmond, CA); human tau-specific rabbit polyclonal anti-tau, H150; human tau-specific mouse monoclonal anti-tau HT7; phosphorylation-dependent mouse monoclonal anti-tau AT180 (Innogenetics Zwijndrecht, Belgium), which recognizes tau phosphorylated at Ser231; AT8 (Innogenetics Zwijndrecht, Belgium), which recognizes tau phosphorylated at Ser202 and Ser205; and PHF-1 (generously provided by Dr Peter Davies, Albert Einstein College of Medicine, NY), which recognizes tau phosphorylated at Ser396 and Ser404.

Western blotting

Mouse brains were homogenized in TBS (10 mM Tris, 150 mM NaCl, pH7.4) containing protease inhibitors (1 μg/ml antipine, 5 μg/ml pepstatin, 5 μg/ml leupeptin, 2 μg/ml aprotinin, and 0.5 μM 4-(2-aminoethyl)benzenesulfonyl fluoride hydrochloride) and phosphatase inhibitors (1 mM NaF, 0.4 μM Na_3VO_4, and 0.5 μM okadaic acid). After centrifugation at 27 000 *g* for 20 min, the supernatant was collected. Sarcosyl-insoluble, paired helical filament-enriched fractions were prepared from TBS-insoluble pellets. The resulting precipitate was re-homogenized in 5 volumes of 0.8 M NaCl and 10% sucrose solution and centrifuged at 27 000 *g* for 20 min. One-tenth volume of 10% sarcosyl solution was added to the supernatant, which was then mixed by vortex, incubated for 1 h at 37°C, and centrifuged at 150 000 *g* for 1 h. The resulting pellet was analyzed as the sarcosyl-insoluble fraction. TBS-soluble and sarcosyl-insoluble materials were solubilized in Laemmli sample buffer and subjected to SDS–PAGE. Separated proteins were blotted onto nitrocellulose membranes (Schleicher & Schuell Bioscience, Dassel, Germany). The membranes were incubated with primary antibody, followed by the appropriate-species HRP-conjugated secondary antibody. Chemiluminescent detection (ECL, GE Healthcare Bio Science) was used for visualization. Quantitation and visual analysis of immunoreactivity were performed with a computer-linked LAS-3000 Bio-Imaging Analyzer System (Fujifilm).

Histology and immunohistochemical procedures

Mice were deeply anesthetized with pentobarbital (50 mg/kg), then transcardially perfused with 10% formalin. Brains were postfixed in the same fixative for 16 h and embedded in paraffin and sectioned (4–6 μm) in the coronal plane. Deparaffinized sections were treated with Target Retrieval Solution (Dako) for 20 min at 80°C, blocked in 0.1% BSA/TBS, and incubated with primary antibodies in 0.1% BSA/TBS overnight at 4°C. A fluorescent microscope equipped with a cooled CCD camera and Neurolucida software (version 7; MicroBrightField Inc., USA) were used to analyze the sections and for acquisition of images under virtual slice mode. Golgi staining was performed with an FD Rapid GolgiStain™ kit (FD Neuro Technologies, MD, USA).

Morris water maze test

To assess place learning and memory performance of Wtau-Tg mice, we used a cylindrical test apparatus (1 m in diameter) and task fashioned after the Morris water maze. The water was maintained at 24°C, and the maze was surrounded by landmark objects. A slightly submerged transparent platform, to which the mice could escape, was hidden from view by making the water opaque with a white bio-safe material. The position of the platform was fixed during a 60 s test period.

Mouse behavior during the water maze test was monitored by a CCD camera mounted overhead; digital data of real-time images were recorded to a PC using the public domain NIH Image program (developed at The National Institute of Mental Health and available on the Internet at http://rsb.info.nih.gov/nih-image/). Images were sampled at 2 Hz. Data were analyzed using customized software based on Matlab (version 7.2, Mathworks Co Ltd, CA) with image analysis tool box (Mathworks Co Ltd, CA). During testing, the sequential position of the mouse was determined in each video frame, and the swimming speed, distance from platform, and latency to reach the platform were calculated. To assess learning, for each mouse, we measured the distance between the mouse and the platform every 0.5 s until the mouse reached the platform. Next, we calculated the total distance traveled by the mouse by integrating the distance between the mouse and the platform. This 'integral distance' value represents the error score. We used this error score as a measure of learning performance.

For learning trials, the mouse was gently placed on the water surface close to the cylinder wall in the opposite half of the maze away from the platform; it was allowed to swim freely for a 60 s test period. When the mouse did not escape to the submerged platform within this test period, we gently navigated it to the platform by hand and made it stay there for 20 s. For each mouse, we carried out three learning trials per day for 9 successive days. A single probe test was given on the 10th day, in which the platform was removed from the maze in the mouse's absence. The mouse was introduced into the maze as before and allowed to search for the missing platform for 60 s.

The maze surface was logically partitioned into quadrants for analysis, and the percentage of time that the mouse spent searching in each quadrant was calculated. This percentage was used as an index of memory performance, the logic being that if the mouse remembered where the platform was during training, it would spend a disproportionate percentage of its swimming time during the probe trial searching in the quadrant, where the platform was located during the learning trials. An error score for the probe test was calculated by measuring the total distance the mouse traveled for 60 s. Statistical analyses were conducted using PRISM4 (GraphPad Software Inc., CA). Data were analyzed using the Friedman test or two-way ANOVA, unless noted otherwise.

Mn-enhanced MRI

MR scanning of mouse brains was performed using a vertical-bore 9.4 T Bruker AVANCE 400WB imaging spectrometer with a 250 mTm-1 actively shielded imaging gradient insert (Bruker BioSpin). The image of T1-weighted gradient-echo 3D 1H magnetic resonance was obtained at 400 MHz radio-frequency pulses. The parameters for obtaining images were as follows: TE = 5 ms; TR = 50 ms; matrix dimensions = 256 × 256 × 256 (resolution = 100 × 100 × 100 μm); and scanning time per sample = 54 min.

The density of the enhanced MR signal depended on the concentration of $MnCl_2$ (Supplementary Figure 2A, B). We injected each mouse intraperitoneally with a 30 mM $MnCl_2$ solution (100 μM/kg) and placed the mouse in its home cage for 4 h before MR scanning. We used this concentration of $MnCl_2$ because higher concentrations affect locomotor activity. Next, the mouse was exposed successively to three different novel places separated by a transparent plastic wall (circular open field, 60 cm in diameter) and was allowed to explore for 120 min. After exposing the mouse to the novel environments, the mouse was returned to its home cage for

1 h. It was anesthetized with a pentobarbital solution (dose: 50 mg/kg, i.p.) before MRI. Comparison of MR images obtained from mice exposed only to their home cage to those obtained from mice exposed to novel environments revealed that the latter increased MEM signals in olfactory cortex (piriform cortex), somatosensory area, and the parahippocampal area (perirhinal, postrhinal, and entorhinal cortices) (Supplementary Figure 2C, D).

During MR scanning, the mouse's breathing and depth of anesthesia was monitored with a sensor. Breathing rate was maintained at 80–100 breaths per min and anesthesia was maintained with 0.5–1.5% isoflurane mixed in air. Raw MRI data (16 bit) were analyzed with a PowerMac G5 Macintosh Computer and Matlab-based custom software. MEM images were visualized with Osirix version 2.5, an open-source software program for navigating multidimensional DICOM images (Rosset *et al*, 2004). First, brain slices were ordered in sequential rostrocaudal order and aligned based on bregma positions using custom software. Second, all voxel data in the aligned and stacked slices were smoothed using a three-dimensional Gaussian filter (Matlab image processing tool box, version 5.02, Mathworks). Finally, relative regional brain activity was determined by measuring MR signal intensities in different parahippocampal cortical regions and normalizing these intensities by the mean signal intensity in the dorsal striatum, according to the method of Yu *et al* (2005).

Flat map analysis

To compare cortical activity from different animals, we generated two-dimensional, cortical flat maps showing the distribution of neural activity in cortical regions adjacent to the rhinal fissure. We mainly analyzed neural activity in temporal, postrhinal, perirhinal, entorhinal, and piriform cortices. These maps were derived from individual, serial coronal slices obtained from MEM imaging as follows (Supplementary Figure 3). First, for each serial coronal slice, we identified edge pixels demarcating the surface of the brain; edge pixels were identified according to signal intensity. Because we were primarily interested in analyzing activity in parahippocampal areas, we identified only edge pixels located 30 pixels above and below the rhinal fissure. Second, we identified guide pixels representing the average MEM signal intensity 300 μm just deep to the edge pixels. MEM signals can be detected as deep as 500 μm from the brain surface; thus, it is conceivable that activity in deep layers of cortex can also be detected. We identified only guide pixels located 30 pixels above and below the rhinal fissure. A map was constructed by stacking the segments of guide pixels of each section onto a template of equally spaced straight lines. These segments were aligned along the rhinal fissure. Finally, we plotted regional cortical activity, which we defined as the average intensity found within 5 pixels of each guide pixel, onto the two-dimensional flat maps.

The flat maps also enabled us to compare cortical activities in non-Tg and Wtau-Tg mice using statistical analysis. First, we constructed flat maps containing the average neural activity of 4–6 aged non-Tg and Wtau-Tg mice. Because individual mice within these two groups showed small error score differences (see Figure 3), we combined neural activity data from aged non-Tg and Wtau-Tg mice for our correlation analysis.

We then calculated correlation coefficients (R^2) for data from each animal to determine the relationship between neural activity in different brain regions and memory performance and evaluated the accuracy of these coefficients by calculating Pearson's probability. R^2 values were plotted onto the flat map only when statistical significance ($P<0.01$) was detected. To reduce statistical noise produced by multiple comparisons, a special filter (3×3 box) was applied.

To compare cortical PHF1 immunoreactivity to the correlation coefficients analysis of neural activity and memory performance, we generated flat maps showing the spatial distribution of PHF1 immunoreactivity in aged Wtau-Tg mice. These maps were based on fluorescent images obtained from six serial coronal sections (300 μm apart), which were obtained by a CCD camera at the same spatial resolution as that of the MEM images (100 μm^2 pixel). Immunoreactivity intensity was mapped as described above (see Supplementary Figure 3). Then, the rostrocaudal resolution of the PHF1 map was modified by linear interpolation using Matlab software to compare it to MRI flat maps.

Supplementary data

Supplementary data are available at *The EMBO Journal* Online (http://www.embojournal.org).

Acknowledgements

This work is partly supported by Grant-Aid for Scientific Research on Priority Areas, Research on Pathomechanism of Brain Disorder, from the Ministry of Education, Culture, Sports, Science and Technology of Japan.

References

Alonso AC, Grundke-Iqbal I, Iqbal K (1996) Alzheimer's disease hyperphosphorylated tau sequesters normal tau into tangles of filaments and disassembles microtubules. *Nat Med* **2:** 783–787

Alonso AC, Li B, Grundke-Iqbal I, Iqbal K (2006) Polymerization of hyperphosphorylated tau into filaments eliminates its inhibitory activity. *Proc Natl Acad Sci USA* **103:** 8864–8869

Alonso AC, Zaidi T, Grundke-Iqbal I, Iqbal K (1994) Role of abnormally phosphorylated tau in the breakdown of microtubules in Alzheimer disease. *Proc Natl Acad Sci USA* **91:** 5562–5566

Alonso AC, Grundke-Iqbal I, Barra HS, Iqbal K (1997) Abnormal phosphorylation of tau and the mechanism of Alzheimer neurofibrillary degeneration: sequestration of microtubule-associated proteins 1 and 2 and the disassembly of microtubules by the abnormal tau. *Proc Natl Acad Sci USA* **94:** 298–303

Andorfer C, Acker CM, Kress Y, Hof PR, Duff K, Davies P (2005) Cell-cycle reentry and cell death in transgenic mice expressing nonmutant human tau isoforms. *J Neurosci* **25:** 5446–5454

Bancher C, Brunner C, Lassmann H, Budka H, Jellinger K, Seitelberger F, Grundke-Iqbal I, Iqbal K, Wisniewski HM (1989) Tau and ubiquitin immunoreactivity at different stages of formation of Alzheimer neurofibrillary tangles. *Prog Clin Biol Res* **317:** 837–848

Binder LI, Guillozet-Bongaarts AL, Garcia-Sierra F, Berry RW (2005) Tau, tangles, and Alzheimer's disease. *Biochim Biophys Acta* **1739:** 216–223

Braak H, Braak E (1991) Neuropathological stageing of Alzheimer-related changes. *Acta Neuropathol (Berl)* **82:** 239–259

Chapman PF, White GL, Jones MW, Cooper-Blacketer D, Marshall VJ, Irizarry M, Younkin L, Good MA, Bliss TV, Hyman BT, Younkin SG, Hsiao KK (1999) Impaired synaptic plasticity and learning in aged amyloid precursor protein transgenic mice. *Nat Neurosci* **2:** 271–276

Chen G, Chen KS, Knox J, Inglis J, Bernard A, Martin SJ, Justice A, McConlogue L, Games D, Freedman SB, Morris RG (2000) A learning deficit related to age and beta-amyloid plaques in a mouse model of Alzheimer's disease. *Nature* **408:** 975–979

Ebneth A, Godemann R, Stamer K, Illenberger S, Trinczek B, Mandelkow E (1998) Overexpression of tau protein inhibits kinesin-dependent trafficking of vesicles, mitochondria, and endoplasmic reticulum: implications for Alzheimer's disease. *J Cell Biol* **143:** 777–794

Egashira N, Iwasaki K, Takashima A, Watanabe T, Kawabe H, Matsuda T, Mishima K, Chidori S, Nishimura R, Fujiwara M (2005) Altered depression-related behavior and neurochemical changes in serotonergic neurons in mutant R406W human tau transgenic mice. *Brain Res* **1059:** 7–12

Goedert M, Spillantini MG (2000) Tau mutations in frontotemporal dementia FTDP-17 and their relevance for Alzheimer's disease. *Biochim Biophys Acta* **1502:** 110–121

Gomez-Isla T, Hollister R, West H, Mui S, Growdon JH, Petersen RC, Parisi JE, Hyman BT (1997) Neuronal loss correlates with but exceeds neurofibrillary tangles in Alzheimer's disease. *Ann Neurol* **41:** 17–24

Gotz J, Barmettler R, Ferrari A, Goedert M, Probst A, Nitsch RM (2000) *In vivo* analysis of wild-type and FTDP-17 tau transgenic mice. *Ann N Y Acad Sci* **920:** 126–133

Gotz J, Chen F, van Dorpe J, Nitsch RM (2001) Formation of neurofibrillary tangles in P301l tau transgenic mice induced by Abeta 42 fibrils. *Science* **293:** 1491–1495

Gotz J, Streffer JR, David D, Schild A, Hoerndli F, Pennanen L, Kurosinski P, Chen F (2004) Transgenic animal models of Alzheimer's disease and related disorders: histopathology, behavior and therapy. *Mol Psychiatry* **9:** 664–683

Hafting T, Fyhn M, Molden S, Moser MB, Moser EI (2005) Microstructure of a spatial map in the entorhinal cortex. *Nature* **436:** 801–806

Hedden T, Gabrieli JD (2004) Insights into the ageing mind: a view from cognitive neuroscience. *Nat Rev Neurosci* **5:** 87–96

Hedden T, Gabrieli JD (2005) Healthy and pathological processes in adult development: new evidence from neuroimaging of the aging brain. *Curr Opin Neurol* **18:** 740–747

Hutton M (2000) Molecular genetics of chromosome 17 tauopathies. *Ann N Y Acad Sci* **920:** 63–73

Iqbal K, Grundke-Iqbal I (2005) Metabolic/signal transduction hypothesis of Alzheimer's disease and other tauopathies. *Acta Neuropathol (Berl)* **109:** 25–31

Iqbal K, Grundke-Iqbal I, Wisniewski HM (1986) Neuronal cytoskeleton in aging and dementia. *Prog Brain Res* **70:** 279–288

Ishihara T, Zhang B, Higuchi M, Yoshiyama Y, Trojanowski JQ, Lee VM (2001) Age-dependent induction of congophilic neurofibrillary tau inclusions in tau transgenic mice. *Am J Pathol* **158:** 555–562

Kopke E, Tung YC, Shaikh S, Alonso AC, Iqbal K, Grundke-Iqbal I (1993) Microtubule-associated protein tau. Abnormal phosphorylation of a non-paired helical filament pool in Alzheimer disease. *J Biol Chem* **268:** 24374–24384

Lalonde R, Dumont M, Staufenbiel M, Sturchler-Pierrat C, Strazielle C (2002) Spatial learning, exploration, anxiety, and motor coordination in female APP23 transgenic mice with the Swedish mutation. *Brain Res* **956:** 36–44

Lavenex P, Amaral DG (2000) Hippocampal–cortical interaction: a hierarchy of associativity. *Hippocampus* **10:** 420–430

Lee VM, Goedert M, Trojanowski JQ (2001) Neurodegenerative tauopathies. *Annu Rev Neurosci* **24:** 1121–1159

Lee VM, Kenyon TK, Trojanowski JQ (2005) Transgenic animal models of tauopathies. *Biochim Biophys Acta* **1739:** 251–259

Lewis J, Dickson DW, Lin WL, Chisholm L, Corral A, Jones G, Yen SH, Sahara N, Skipper L, Yager D, Eckman C, Hardy J, Hutton M, McGowan E (2001) Enhanced neurofibrillary degeneration in transgenic mice expressing mutant tau and APP. *Science* **293:** 1487–1491

Lewis J, McGowan E, Rockwood J, Melrose H, Nacharaju P, Van Slegtenhorst M, Gwinn-Hardy K, Paul Murphy M, Baker M, Yu X, Duff K, Hardy J, Corral A, Lin WL, Yen SH, Dickson DW, Davies P, Hutton M (2000) Neurofibrillary tangles, amyotrophy and progressive motor disturbance in mice expressing mutant (P301L) tau protein. *Nat Genet* **25:** 402–405

Maeda S, Sahara N, Saito Y, Murayama M, Yoshiike Y, Kim H, Miyasaka T, Murayama S, Ikai A, Takashima A (2007) Granular tau oligomers as intermediates of tau filaments. *Biochemistry* **46:** 3856–3861

Maeda S, Sahara N, Saito Y, Murayama S, Ikai A, Takashima A (2006) Increased levels of granular tau oligomers: an early sign of brain aging and Alzheimer's disease. *Neurosci Res* **54:** 197–201

McNaughton BL, Battaglia FP, Jensen O, Moser EI, Moser MB (2006) Path integration and the neural basis of the 'cognitive map'. *Nat Rev Neurosci* **7:** 663–678

Morris RG (2006) Elements of a neurobiological theory of hippocampal function: the role of synaptic plasticity, synaptic tagging and schemas. *Eur J Neurosci* **23:** 2829–2846

Murakami T, Paitel E, Kawarabayashi T, Ikeda M, Chishti MA, Janus C, Matsubara E, Sasaki A, Kawarai T, Phinney AL, Harigaya Y, Horne P, Egashira N, Mishima K, Hanna A, Yang J, Iwasaki K, Takahashi M, Fujiwara M, Ishiguro K *et al* (2006) Cortical neuronal and glial pathology in TgTauP301L transgenic mice: neuronal degeneration, memory disturbance, and phenotypic variation. *Am J Pathol* **169:** 1365–1375

Oddo S, Caccamo A, Shepherd JD, Murphy MP, Golde TE, Kayed R, Metherate R, Mattson MP, Akbari Y, LaFerla FM (2003) Triple-transgenic model of Alzheimer's disease with plaques and tangles: intracellular Abeta and synaptic dysfunction. *Neuron* **39:** 409–421

Ramsden M, Kotilinek L, Forster C, Paulson J, McGowan E, SantaCruz K, Guimaraes A, Yue M, Lewis J, Carlson G, Hutton M, Ashe KH (2005) Age-dependent neurofibrillary tangle formation, neuron loss, and memory impairment in a mouse model of human tauopathy (P301L). *J Neurosci* **25:** 10637–10647

Rosset A, Spadola L, Ratib O (2004) Osirix: an open-source software for navigating in multidimensional DICOM images. *J Dig Image* **7:** 205–216

Rypma B, Prabhakaran V, Desmond JE, Gabrieli JD (2001) Age differences in prefrontal cortical activity in working memory. *Psychol Aging* **16:** 371–384

Santacruz K, Lewis J, Spires T, Paulson J, Kotilinek L, Ingelsson M, Guimaraes A, DeTure M, Ramsden M, McGowan E, Forster C, Yue M, Orne J, Janus C, Mariash A, Kuskowski M, Hyman B, Hutton M, Ashe KH (2005) Tau suppression in a neurodegenerative mouse model improves memory function. *Science* **309:** 476–481

Santarella RA, Skiniotis G, Goldie KN, Tittmann P, Gross H, Mandelkow EM, Mandelkow E, Hoenger A (2004) Surface-decoration of microtubules by human tau. *J Mol Biol* **339:** 539–553

Seitz A, Kojima H, Oiwa K, Mandelkow EM, Song YH, Mandelkow E (2002) Single-molecule investigation of the interference between kinesin, tau and MAP2c. *EMBO J* **21:** 4896–4905

Spillantini MG, Van Swieten JC, Goedert M (2000) Tau gene mutations in frontotemporal dementia and parkinsonism linked to chromosome 17 (FTDP-17). *Neurogenetics* **2:** 193–205

Spires TL, Orne JD, SantaCruz K, Pitstick R, Carlson GA, Ashe KH, Hyman BT (2006) Region-specific dissociation of neuronal loss and neurofibrillary pathology in a mouse model of tauopathy. *Am J Pathol* **168:** 1598–1607

Stamer K, Vogel R, Thies E, Mandelkow E, Mandelkow EM (2002) Tau blocks traffic of organelles, neurofilaments, and APP vesicles in neurons and enhances oxidative stress. *J Cell Biol* **156:** 1051–1063

Steffenach HA, Witter M, Moser MB, Moser EI (2005) Spatial memory in the rat requires the dorsolateral band of the entorhinal cortex. *Neuron* **45:** 301–313

Takashima A (2006) GSK-3 is essential in the pathogenesis of Alzheimer's disease. *J Alzheimers Dis* **9:** 309–317

Tanemura K, Akagi T, Murayama M, Kikuchi N, Murayama O, Hashikawa T, Yoshiike Y, Park JM, Matsuda K, Nakao S, Sun X, Sato S, Yamaguchi H, Takashima A (2001) Formation of filamentous tau aggregations in transgenic mice expressing V337M human tau. *Neurobiol Dis* **8:** 1036–1045

Tanemura K, Murayama M, Akagi T, Hashikawa T, Tominaga T, Ichikawa M, Yamaguchi H, Takashima A (2002) Neurodegeneration with tau accumulation in a transgenic mouse expressing V337M human tau. *J Neurosci* **22:** 133–141

Taniguchi T, Doe N, Matsuyama S, Kitamura Y, Mori H, Saito N, Tanaka C (2005) Transgenic mice expressing mutant (N279K) human tau show mutation dependent cognitive deficits without neurofibrillary tangle formation. *FEBS Lett* **579:** 5704–5712

Tatebayashi Y, Miyasaka T, Chui DH, Akagi T, Mishima K, Iwasaki K, Fujiwara M, Tanemura K, Murayama M, Ishiguro K, Planel E, Sato S, Hashikawa T, Takashima A (2002) Tau filament formation and associative memory deficit in aged mice expressing mutant (R406W) human tau. *Proc Natl Acad Sci USA* **99:** 13896–13901

Van Dam D, D'Hooge R, Staufenbiel M, Van Ginneken C, Van Meir F, De Deyn PP (2003) Age-dependent cognitive decline in the APP23 model precedes amyloid deposition. *Eur J Neurosci* **17:** 388–396

Wadghiri YZ, Blind JA, Duan X, Moreno C, Yu X, Joyner AL, Turnbull DH (2004) Manganese-enhanced magnetic resonance imaging (MEMRI) of mouse brain development. *NMR Biomed* **17:** 613–619

Wang JZ, Grundke-Iqbal I, Iqbal K (2007) Kinases and phosphatases and tau sites involved in Alzheimer neurofibrillary degeneration. *Eur J Neurosci* **25:** 59–68

Yoshiyama Y, Uryu K, Higuchi M, Longhi L, Hoover R, Fujimoto S, McIntosh T, Lee VM, Trojanowski JQ (2005) Enhanced neurofibrillary tangle formation, cerebral atrophy, and cognitive deficits induced by repetitive mild brain injury in a transgenic tauopathy mouse model. *J Neurotrauma* **22:** 1134–1141

Yu X, Wadghiri YZ, Sanes DH, Turnbull DH (2005) *In vivo* auditory brain mapping in mice with Mn-enhanced MRI. *Nat Neurosci* **8:** 961–968

